Krypton Tagging Velocimetry (KTV) Investigation of Shock-Wave/Turbulent Boundary-Layer Interaction

M. A. Mustafa* M. B. Hunt† N. J. Parziale‡
Stevens Institute of Technology, Hoboken, NJ 07030, USA
M. S. Smith§ E. C. Marineau¶
AEDC White Oak, Silver Spring, MD 20903, USA

Seven profiles of streamwise velocity and velocity fluctuations were measured in the incoming boundary layer and immediately upstream of a 24-degree compression corner in a $M_\infty = 2.8$, $\mathbf{Re}_\Theta = 1750$ shock-wave/turbulent boundary-layer interaction. The measurements were made with Krypton Tagging Velocimetry (KTV) in 99% N_2/1% Kr flow. Globally seeding 1% Kr into the flow (premixed N_2/Kr K-bottles from distributor) alters the major non-dimensional transport properties by 0.1-0.3%. The mean-velocity and velocity-fluctuation profiles in the incoming supersonic turbulent boundary layer were found to agree with datasets in the literature, thus, the baseline flow was established. The mean-velocity profiles in the region immediately upstream of the 24-degree compression corner were found to agree with Direct Numerical Simulation (DNS) results available in the literature. In addition, the presence of a shear layer was detected, and its location and orientation are compared to that in the literature.

Nomenclature

γ	Ratio of specific heats, (-)
ρ	Density, (kg/m^3)
P	Pressure, (Pa)
t	Time, (s)
τ	Timescale, (1/s)
T	Temperature, (K)
M	Mach Number, (-)
Re	Reynolds Number, (-)
U	Velocity, (m/s)
u_τ	Friction velocity, (m/s)
x	Distance, (m)
r	Recovery Factor, (-)
Θ	Momentum Thickness
c	Sound speed, (m/s)

Subscript

m	Metastable
∞	Free Stream
Θ	Based on Momentum Thickness
w	Wall

*Graduate Student, Mechanical Engineering, Castle Point on Hudson, Hoboken, New Jersey, 07030.
†Graduate Student, Mechanical Engineering, Castle Point on Hudson, Hoboken, New Jersey, 07030.
‡Assistant Professor, Mechanical Engineering, Castle Point on Hudson, Hoboken, New Jersey, 07030, AIAA Member.
§Senior Research Engineer, National Aerospace Solutions, Silver Spring, MD 20903, Senior AIAA Member.
¶Chief Technologist, AEDC White Oak, Silver Spring, MD 20903, Senior AIAA Member.

I. Introduction

The need to accurately assess the heat transfer, skin friction, and velocity profiles on high-speed vehicles is motivated by a recent push for operationally-responsive space access and conventional prompt global strike (CPGS).[1–3] To more clearly understand the fundamental flow physics about high-speed vehicles, researchers devise and focus effort on canonical or model problems.

This approach has been applied to shock-wave/turbulent boundary-layer interaction. Dolling[4] states "[shock-wave boundary-layer interactions] are ubiquitous in high-speed flight, occurring in an almost limitless number of external and internal flow problems relevant to aircraft, missiles, rockets, and projectiles. Maximum mean and fluctuating pressure levels and thermal loads that a structure is exposed to are generally found in regions of shock/boundary-layer and shock/shear-layer interaction and can effect vehicle and component geometry, structural integrity, material selection, fatigue life, the design of thermal protection systems, weight, and cost." Researchers have made significant experimental investigations,[5–23] computational investigations,[24–32] and reviews[33–39] of the study of shock-wave/boundary-layer interactions, motivated by the pursuit of a fundamental understanding of the flow physics for the purpose of designing robust high-speed vehicles.

An important issue is that state-of-the-art production codes that are typically used to design hypersonic vehicles have difficulty accurately computing shock-wave/boundary-layer interactions with the current suite of turbulence models.[40] In the long term, we aim to make a contribution with krypton tagging velocimetry (KTV) to fill the need for high-fidelity experimental data that characterizes shock-wave/boundary-layer interactions at high Mach number for the development of new modeling methods where other experimental methods may not be appropriate. Particle-based methods of velocimetry, particle-image velocimetry (PIV) in particular, can currently produce high-quality multi-component velocity data.[38] However, the limitations of implementing particle-based techniques in high-speed facilities include timing issues associated with particle injection[41] and reduced particle response at Knudsen and Reynolds numbers[42] typical of high-speed wind tunnels. Timing and seeding issues associated with PIV are technical in nature and may be addressed in certain situations. However, reduced particle response is a fundamental limitation that may not be overcome when attempting to apply PIV in certain flows.

Tagging velocimetry[43] is typically performed in gases by tracking the fluorescence of a native, seeded, or synthesized gas. In contrast to the limitations of implementing PIV techniques in high-speed facilities, the implementation of tagging velocimetry is not limited by timing issues associated with tracer injection[41] or reduced particle response at Knudsen and Reynolds numbers[42] typical of high-speed wind tunnels. Noted methods and tracers of tagging velocimetry include VENOM,[44–48] APART,[49–51] RELIEF,[52–56] FLEET,[57,58] STARFLEET,[59] PLEET,[60] iodine,[61,62] acetone,[63–65] and the hydroxyl group techniques,[66–68] among others.[69–73]

In this paper, we are attempting to establish KTV as a viable method of measurement in the complex flow of shock-wave/turbulent boundary-layer interaction. To achieve this, the baseline flow field is quantified in the form of mean-velocity and fluctuation profiles in the incoming supersonic turbulent boundary layer. Schlieren cinematography and Krypton Planar Laser-Induced Fluorescence results in the flow field about the 24-degree wedge are presented to establish that 1) the Mach 3 AEDC Calibration Tunnel (M3CT) started and 2) the flow field is visibly similar to work in literature so that the problem could be treated as canonical. Finally, mean-velocity and fluctuation profiles for the flow field immediately upstream of the 24-degree compression corner as measured by Krypton Tagging Velocimetry are presented and compared to the literature as appropriate.

II. Krypton Tagging Velocimetry (KTV) Setup

Krypton Tagging Velocimetry (KTV), relative to other tagging velocimetry techniques, relies on a chemically inert tracer. This property may enable KTV to broaden the utility of tagging velocimetry because the technique can be applied in gas flows where the chemical composition is difficult to prescribe or predict. The use of a metastable noble gas as a tagging velocimetry tracer was first suggested by Mills et al.[74] and

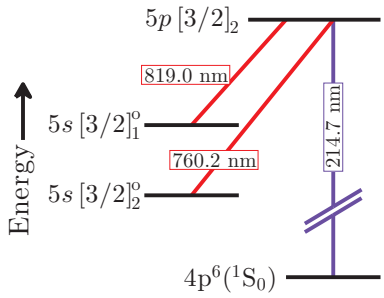

Figure 1. Energy diagram for KTV. Racah nl[K]$_J$ notation.

Balla and Everheart.[75] KTV was first demonstrated by Parziale et al.[76,77] to measure the velocity along the center-line of an underexpanded jet of N_2/Kr mixtures. In that work, pulsed-tunable lasers were used to induce fluorescence of Kr atoms that were seeded into the flow for the purposes of displacement tracking. Following that work, Zahradka et al.[78,79] used KTV to make measurements of the mean and fluctuating profiles in a Mach 2.7 turbulent boundary layer.

The excitation/emission scheme to be used in this work is the same as that of Zahradka et al.[79] Following the energy level diagram (Racah nl[K]$_J$ notation) in Fig. 1, KTV is performed as follows:
1) Seed a base flow with krypton globally.
2) Photosynthesize metastable krypton atoms with a pulsed-tunable laser to form the tagged tracer: two-photon excitation of $4p^6(^1S_0) \rightarrow 5p[3/2]_2$ (214.7 nm) and rapid decay to resonance state $5p[3/2]_2 \rightarrow 5s[3/2]_1^o$ (819.0 nm) and metastable state $5p[3/2]_2 \rightarrow 5s[3/2]_2^o$ (760.2 nm). We estimate that the creation of the metastable atoms which comprise the "write line" takes approximately 50 ns.[80]
3) Record the displacement of the tagged metastable krypton by imaging the laser-induced fluorescence (LIF) that is produced with an additional pulsed-tunable laser: re-excite $5p[3/2]_2$ level by $5s[3/2]_2^o \rightarrow 5p[3/2]_2$ transition with laser sheet (760.2 nm) and read spontaneous emission of $5p[3/2]_2 \rightarrow 5s[3/2]_1^o$ (819.0 nm) transitions with a camera positioned normal to the flow. We estimate that the fluorescence from the Kr tracer occurs for approximately 50 ns after the read-laser pulse. Two high-precision 800 nm longpass filters (Thorlabs FELH0800, transmission of 5e-4% at the read-laser wavelength of 760.2 nm) are placed in series in front of the image intensifier to minimize the noise resulting from the read-laser pulse reflection and scatter from solid surfaces.

The experiment was run using two tunable lasers to provide the 214.7 nm (write) and 760.2 nm (read) laser beams required for KTV (schematic in Fig. 2). The write laser consisted of a frequency doubled Quanta Ray Pro-350 Nd:YAG laser and a frequency tripled Sirah PrecisionScan Dye Laser. The Nd:YAG laser pumped the dye laser with 1000 mJ/pulse at a wavelength of 532 nm. The dye in the laser was DCM[a] with a dimethyl sulfoxide (DMSO) solvent, and the laser was tuned to output a 644.1 nm beam. Frequency tripling of the dye-laser output was performed using Sirah tripling optics (THU 205).

The write-laser beam setup resulted in approximately 10 mJ/pulse, with a wavelength of 214.7 nm, a linewidth of approximately 0.045 cm^{-1}, a pulsewidth of approximately 7 ns, and a repetition rate of 10 Hz. The write-laser beam was directed into the test section with 1 inch 5th-harmonic Nd:YAG laser mirrors (IDEX Y5-1025-45) and focused to several narrow waists into the test section with a 100 mm fused-silica microlens array to form the lines in the streamwise direction and a 100 mm fused-silica cylindrical lens to focus the lines in the spanwise direction.

The read laser consisted of a frequency doubled Quanta Ray Pro-350 Nd:YAG laser and a Sirah PrecisionScan Dye Laser. The Nd:YAG laser pumped the dye laser with 500 mJ/pulse at a wavelength of 532 nm. The dye in the laser was Styryl 8 with a DMSO solvent, and the laser was tuned to output a 760.15 nm beam.

The read-laser beam setup resulted in approximately 50 mJ/pulse, with a wavelength of 760.15 nm, a linewidth of approximately 0.025 cm^{-1}, a pulsewidth of approximately 7 ns, and a repetition rate of 10 Hz. The read-laser beam was directed into the test section using 2 inch broadband dielectric mirrors (Thorlabs

[a]DCM is the trade name for [2-[2-[4-(dimethylamino)phenyl]ethenyl]-6-methyl-4H- pyran-4-ylidene]-propanedinitrile.

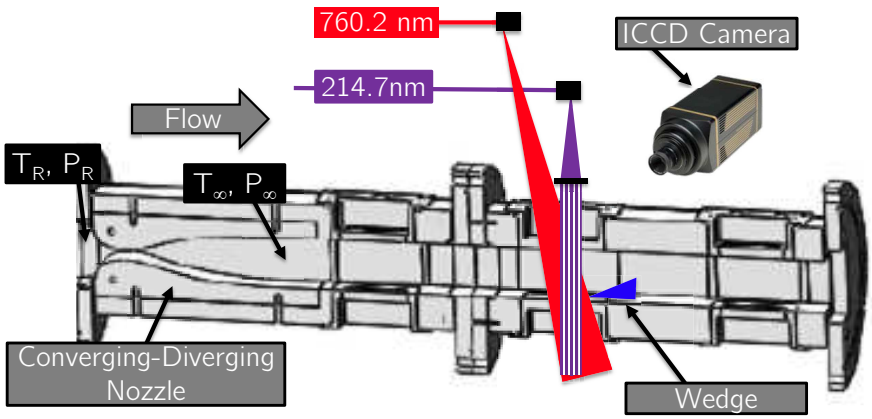

Figure 2. Schematic of experimental setup.

BB2-E02) as a sheet of ≈ 200 µm thickness. This "read sheet" re-excites the metastable Kr tracer atoms so that their displacement can be measured.

The laser and camera timing are controlled by a pulse-delay generator (SRS DG645). The intensified camera used for all experiments is a 16-bit Princeton Instruments PIMAX-4 1024x1024 with an 18-mm grade 1, Gen III extended red filmless intensifier w/ P46 phosphor (PM4-1024i-HR-FG-18-P46-CM). The gain is set to 100% with 2x2 pixel binning to ensure a 10 Hz frame rate. The lens used is a Nikon NIKKOR 24-85mm f/2.8-4D in "macro" mode and positioned approximately 200 mm from the write/read location. Two high-precision 800 nm longpass filters (Thorlabs FELH0800, transmission of 5e-4% at the read-laser wavelength of 760.2 nm) are placed in series between the lens and the intensifier to minimize the noise resulting from the read-laser pulse reflection and scatter from solid surfaces. This was done to enable the imaging of fluorescing Kr atoms near the wind tunnel wall. The camera gate was opened for 50 ns immediately following the read-laser pulse to capture the spontaneous emission of $5p[3/2]_2 \rightarrow 5s[3/2]_1^o$ (819.0 nm) transitions. The KTV measurements are made ≈ 530 mm and ≈ 280 mm from the nozzle throat and nozzle exit, respectively; this is the location of the "Port 2" in the test section (Figs. 2 and 3).

III. Mach 3 AEDC Calibration Tunnel (M3CT) and Run Conditions

The Mach 3 AEDC Calibration Tunnel (M3CT) is an in-draft tunnel often used to test measurement approaches being considered for use in AEDC Hypervelocity Tunnel 9 (T9), which is a large-scale N_2 blow-down hypersonic wind tunnel.[81] The M3CT is a large vacuum tank with a converging-diverging nozzle attached to it. To start the tunnel, a valve is cycled downstream of the nozzle throat. A sketch is shown as Fig. 3, with dimensions in millimeters. To prescribe the freestream Reynolds number, the effective reservoir pressure is modified by choking the flow upstream of the throat with an orifice plate. An isolation bag is added to the end of the tube over the orifice plate which isobarically isolates the test gas from the ambient air in the laboratory. The bag is flexible, so the test gas in the isolation bag is at constant ambient pressure throughout an experiment.

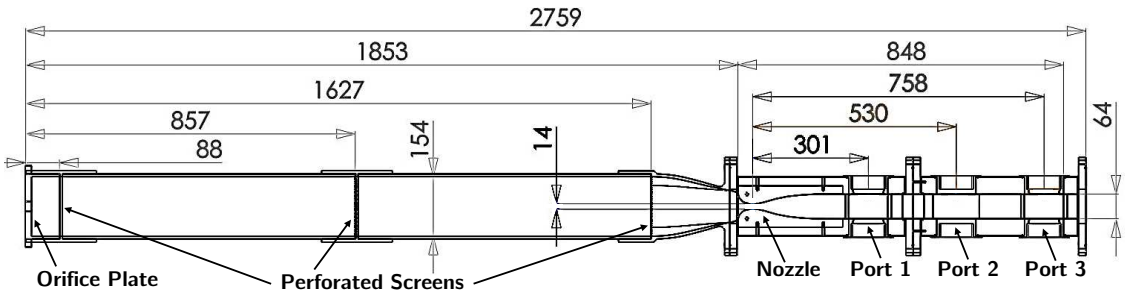

Figure 3. Sketch of AEDC Mach 3 Calibration Tunnel (M3CT). Dimensions in millimeters. The measurements are made at "Port 2."

Table 1. M_∞, P_∞, T_∞, ρ_∞, $\mathrm{Re}_\infty^{unit}$, Re_Θ, and U_∞ are the Mach number, pressure, temperature, density, unit Reynolds number, momentum-thickness Reynolds number, and velocity for each experiment. τ_m and x_m are the calculated time and distance scale, respectively, for the decay of the metastable Kr state.

Experiment	M_∞ (-)	P_∞ (Pa)	T_∞ (K)	ρ_∞ (kg/m^3)	$\mathrm{Re}_\infty^{unit}$ (1/m)	Re_Θ (-)	U_∞ (mm/µs)	$10\tau_m$ (µs)	x_m (mm)
M3 AEDC - 19.1 mm OP	2.77	1010	118	0.030	2.30e6	1750	0.612	4.1	2.5
AEDC Tunnel 9 Run Cond A	9.87	624	53.1	0.040	15.7e6	-	1.466	3.1	4.4
AEDC Tunnel 9 Run Cond B	14.2	311	51.6	0.013	11.7e6	-	2.074	5.9	12.2

Methods for calculating the run conditions and metastable Kr lifetimes can be found in Zahradka et al.[79] Freestream conditions are listed in Table 1. Included in Table 1 are the expected metastable Kr lifetimes, τ_m, and length scales, x_m, for the work presented here and for two representative AEDC Tunnel 9 conditions. The longer the time and length scales, the higher the SNR of the KTV technique. The hypothesis is: if KTV measurements of complex flows can be made in M3CT conditions where quenching of the metastable state is acceptable, then KTV may be applied in T9 where the time and length scales are calculated to be longer than in M3CT.

IV. Flow Visualization in M3CT for $M_\infty = 2.8$, $\mathrm{Re}_\Theta = 1750$ Flow Over 24-Degree Wedge

To ensure that the M3CT started properly and to visualize the shock-wave/turbulent boundary-layer interaction structures, a Z-type schlieren setup[82] and Kr Planar Laser-Induced Fluorescence (KPLIF)[83] were used to visualize the flow field over the 24-degree wedge.

The schlieren setup consisted of a Cavilux HF light source and a Vision Research Phantom v2511 Camera recording at 50k frames-per-second with a 50 ns exposure time. The knife-edge was set as a horizontal cutoff. The first five frames of Fig. 4 are exposures of the schlieren visualization. The last frame in Fig. 4, on the bottom right, is a mean of 3000 images. The purpose of recording this image is to observe the mean shock-wave location and angle. We find the mean shock-wave location and angle ($\approx 32°$) to be approximately the same as experimental data from Settles et al.[5] and DNS data from Priebe and Martin.[30] In a following section, we will overlay KTV results with the mean schlieren exposure.

To visualize structures in the boundary layer, 100% Kr was locally seeded into the boundary layer at "Port 1" in Fig. 3. The injector is of the same design as that in Brooks et al.,[84–86] where care was taken to minimize the disturbance of the mean flow. Then, at "Port 2" a sheet of 214.7 nm light is pulsed (the write pulse from the KTV strategy) in the vicinity of the area just before the wedge for comparison to the schlieren exposures. That is, two-photon excitation of $4p^6(^1\mathrm{S}_0) \rightarrow 5p[3/2]_2$ (214.7 nm) and rapid decay to resonance state $5p[3/2]_2 \rightarrow 5s[3/2]_1^\circ$ (819.0 nm) and metastable state $5p[3/2]_2 \rightarrow 5s[3/2]_2^\circ$ (760.2 nm). Only the $5p[3/2]_2 \rightarrow 5s[3/2]_1^\circ$ (819.0 nm) transitions are imaged because the 800 nm longpass filter is in place.

Eight frames are shown as Fig. 5. The visualization could provide information similar to that of Wu and Miles,[14] although further investigation and data procession is required. It should be noted that there are appreciable differences in experimental approach: in the present KPLIF experiments, 1% of a noble gas is seeded into the boundary layer, whereas in Wu and Miles,[14] filtered Rayleigh scattering (FRS) was used to visualize contrast in condensation level of CO_2 in the cold Mach 2.5 freestream vs. the warmer boundary layer. The need to condense CO_2 could complicate implementation in high-enthalpy facilities. The repetition rate of the Wu and Miles[14] work was 1 MHz, whereas the current KPLIF experiment is limited to 10 Hz by the pump laser; although, a high-repetition rate laser and camera could enable higher frame rates.

Local seeding of different types of gas (including Kr) was investigated by Arisman et al.[87] In that work, the researchers investigated how different seed gases diffused in high-speed boundary layers. They found that the diffusion was acceptable at typical wind-tunnel time/length scales in high-speed laminar boundary layers. The state of the boundary layer in the current work is turbulent, so the mixing rate would be higher; however, it could be possible for Kr to be applied as a seed gas in laminar boundary layers in different applications.

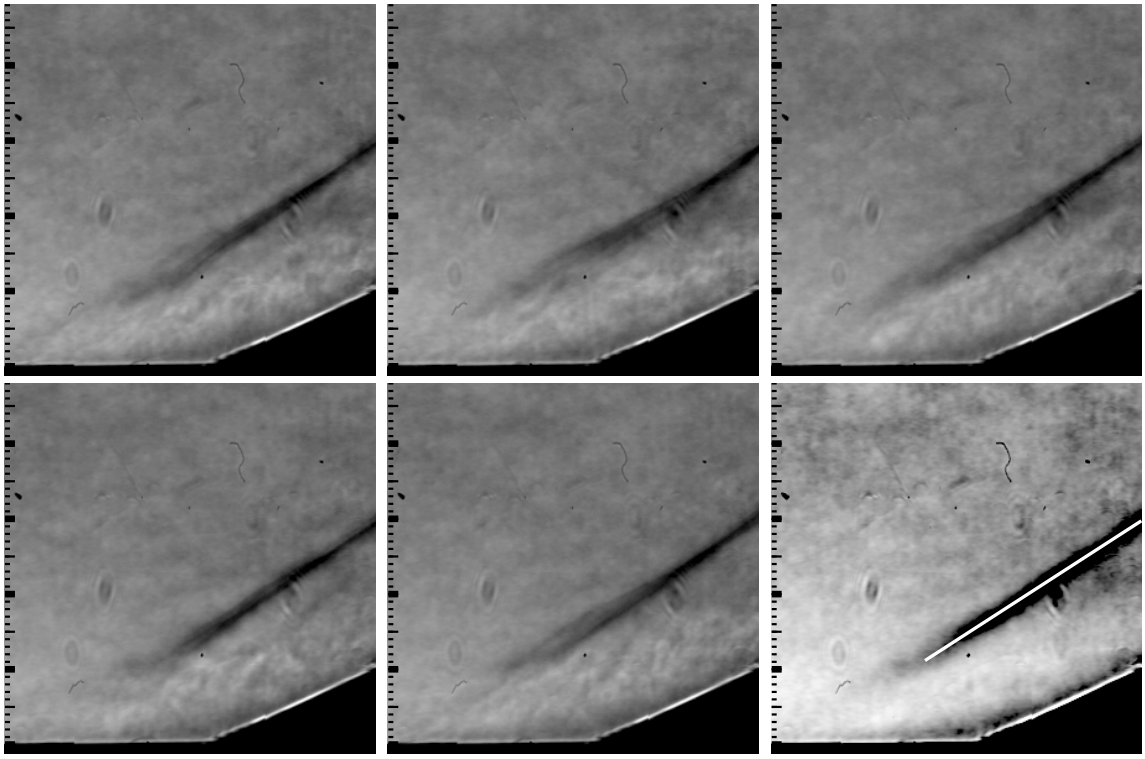

Figure 4. Schlieren of the flow over 24-degree wedge. Flow is left to right. $M_\infty = 2.8$, $\mathrm{Re}_\Theta = 1750$. 50k frames-per-second. 50 ns exposure. Major tick marks at 10 mm. The first five frames are instant exposures, and the image in the bottom right is a mean of 3000 frames. Mean shock location noted by thin white line.

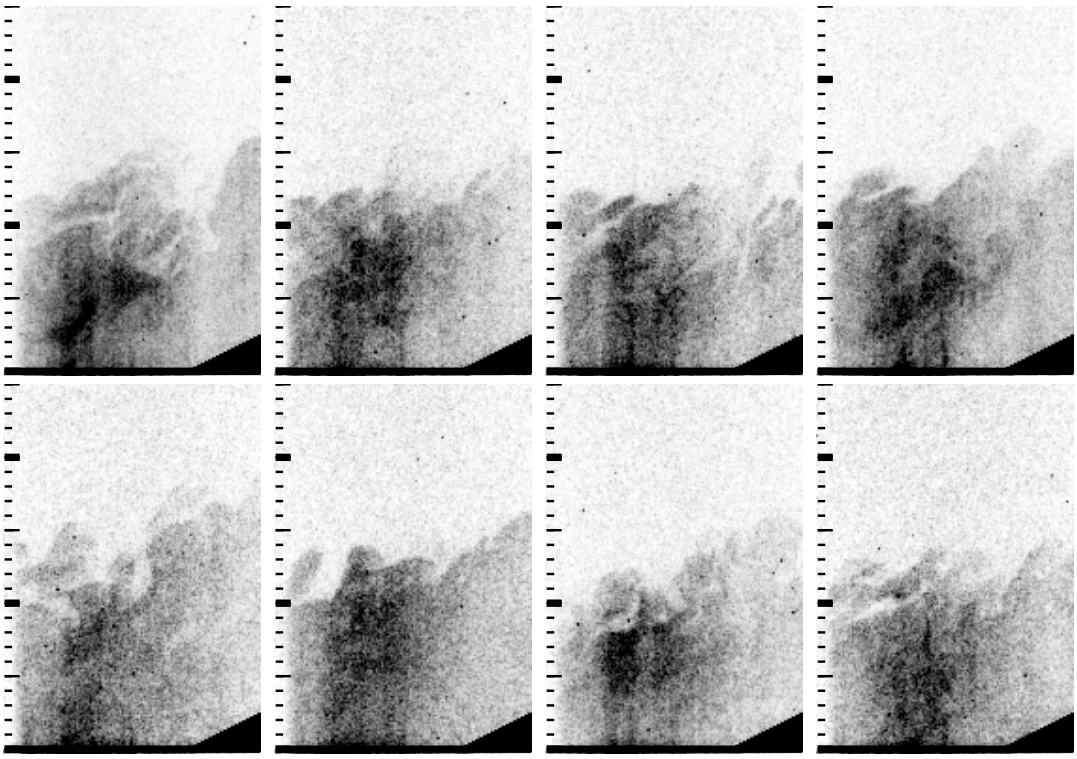

Figure 5. KPLIF of flow over 24-degree wedge. Flow is left to right. Local seeding. $M_\infty = 2.8$, $\mathrm{Re}_\Theta = 1750$. Major tick marks at 10 mm.

In Fig. 5, it is apparent that there is a "hot spot" of the laser sheet in the center of the field of view. This is most likely due to poor beam conditioning. In future work, this would need to be accounted for to make the image sequences of quantitative utility.

Ultimately, the schlieren and KPLIF experiments were intended to establish that the M3CT started and that there were no immediately recognizable defects in the flow. These criteria were met.

V. Multi-Line KTV Boundary-Layer Results in $M_\infty = 2.8$, $\mathbf{Re}_\Theta = 1750$ Flow (No Wedge)

In this section, we present KTV results of streamwise velocity for the $\mathrm{Re}_\Theta = 1750$ case without the 24-degree wedge to establish a baseline boundary-layer profile of streamwise velocity and fluctuations. For the boundary-layer results, the write/read delay was set to 2 µs. The KTV setup formed nine lines, but the middle seven lines were found to consistently yield appropriate SNR. The pulse energy per line was approximately 1 mJ/line. Read exposures are presented as Fig. 6 (top). In Fig. 6 (bot), the exposures are overlaid with the centroid of the tagged Kr after data processing. Large-scale structures can be seen as distortions in successive velocity profiles in the streamwise direction for a single exposure.

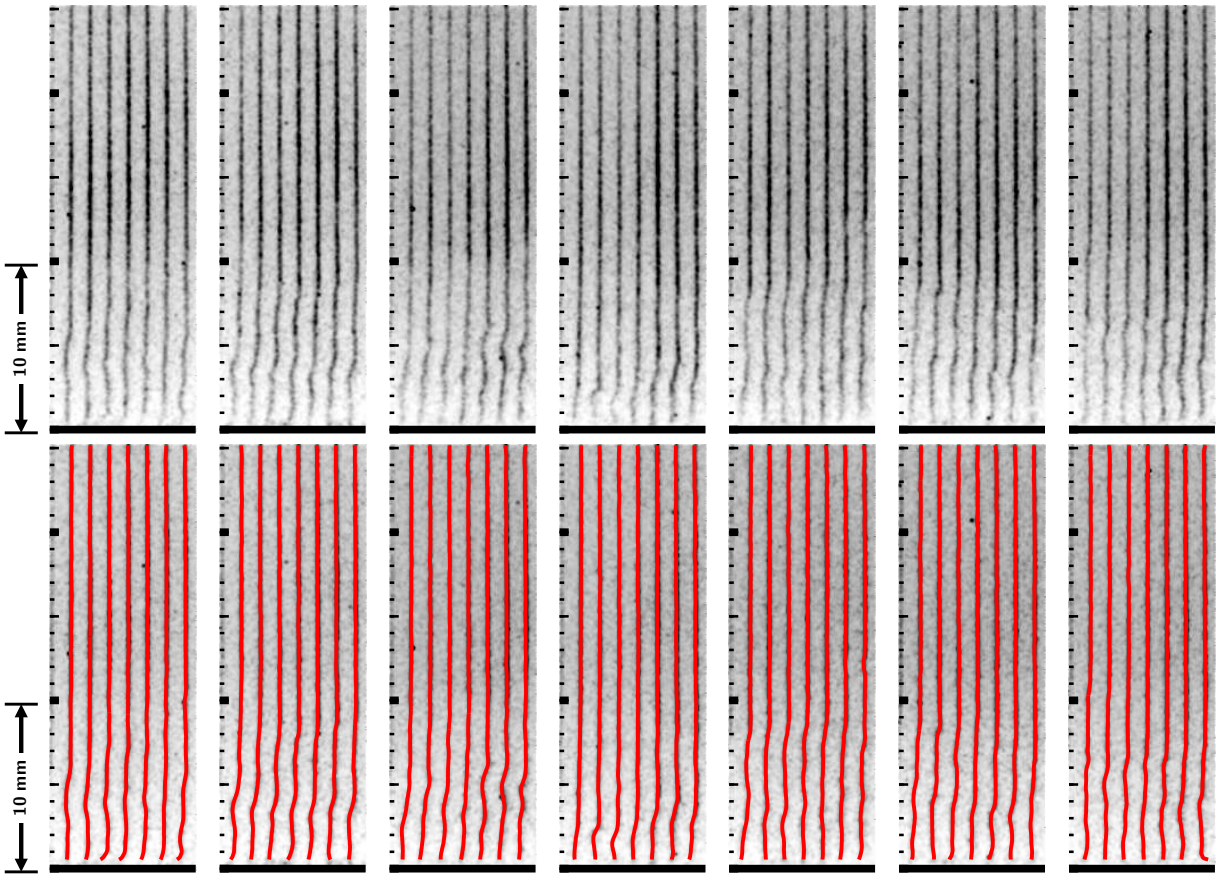

Figure 6. Boundary-layer fluorescence exposures for 7 sample frames. Major tick marks are 10 mm. Flow is left to right. Inverted intensity scale. Wall are masked as black. Top: Exposures, Bottom: Exposures with overlay of Gaussian fits to data.

To process the KTV exposures, the line centers were found in the following way:
1) Crop the image to an appropriate field of view.
2) Apply a two-dimensional Wiener adaptive-noise removal filter.
3) Convert the images to double precision numbers and normalize the intensity to fall in the range of 0-1.
4) Apply the Gaussian peak finding algorithm from O'Haver[88] to find the line centers for the top row using the read lines in the top row of each image as a first guess. This is simple to do in the approximately steady freestream.

5) Proceeding from the top-down, apply the Gaussian peak finding algorithm from O'Haver[88] to find the line centers for each row using the line center location immediately above as the guess.

Steps 4) and 5) are done in parallel in MATLAB for the 500 exposures. The entire process takes approximately 1-2 hours with seven cores on a laptop.

The dimensional velocity is presented in Fig. 7 as measured by KTV from the present work and PIV from Brooks et al.[84–86] in the same facility. Error bars for the KTV measurements are calculated in the same fashion as Zahradka et al.[79] as

$$\delta U_{\mathrm{KTV}} = \left[\left(\delta \Delta x \frac{\partial U}{\partial \Delta x} \right)^2 + \left(\delta \Delta t \frac{\partial U}{\partial \Delta t} \right)^2 + \left(v'_{RMS} \frac{dU}{dy} \Delta t \right)^2 \right]^{\frac{1}{2}}. \tag{1}$$

The uncertainty in the measured displacement distance, Δx, of the metastable tracer is estimated as the 95% confidence bound on the write and read locations from the Gaussian fits. The uncertainty Δt is estimated to be 50 ns, primarily due to fluorescence blurring as considered in Bathel et al.[89] From the manufacturers specification, we estimate that the timing jitter is relatively small, approximately 1 ns for each laser. The fluorescence blurring primarily occurs because of the time scale associated with the 819.0 nm $5p[3/2]_2 \rightarrow 5s[3/2]_1^o$ transition, which is approximately 25 ns;[80,90,91] so, we double this value and report that as the uncertainty in Δt. The third term in Eq. 1 is uncertainty in streamwise velocity due to wall-normal fluctuations in the xy-plane. This formulation is taken from Hill and Klewicki[92] and Bathel et al.[89] The wall-normal fluctuations, v'_{RMS}, are conservatively estimated to be 4% of the edge velocity, which is supported by DNS[29] and PIV experiments.[86]

The error in the KTV measurement is approximately 3% in the freestream, the boundary-layer wake region, and the boundary layer logarithmic region. The error in KTV measurement increases to approximately 8% nearest to the wall. The increase nearest to the wall is mostly due to the third term in Eq. 1. There is an appreciable increase in the wall-normal fluctuations and increase in velocity gradient.

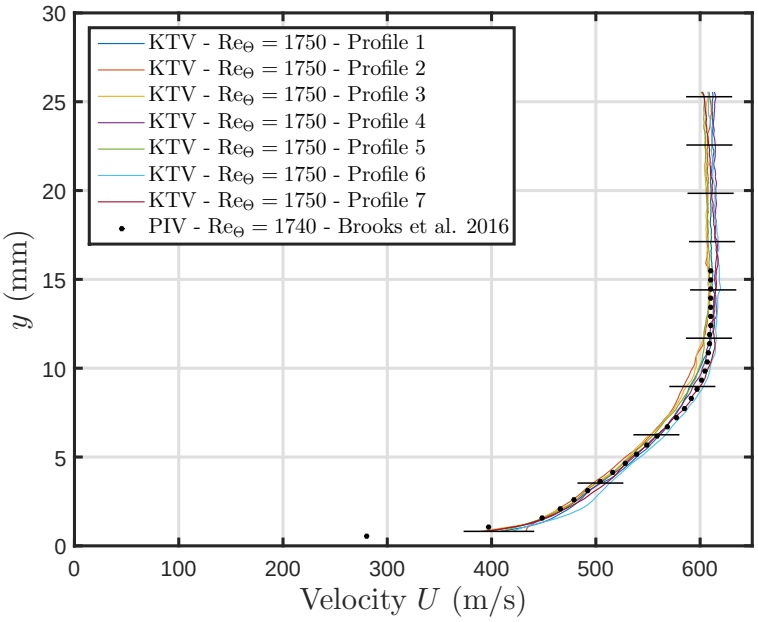

Figure 7. Dimensional velocity of the Mach 2.8 turbulent boundary layer. Error bars in black.

The velocity data from the present study can be compared to the law of the wall in the logarithmic region, $U^+ = \frac{1}{\kappa}\ln(y^+) + C$, by using the Van Driest I transformation, with $y^+ = \rho_w u_\tau y/\mu_w$ and $U^+ = U/u_\tau$. Following Bradshaw[93] and Huang and Coleman,[94] the Van Driest transformed velocity is written as

$$U^+_{VD} = \frac{1}{R}\left[\sin^{-1}\left(\frac{R(U^+ + H)}{\sqrt{1 + R^2 H^2}} \right) - \sin^{-1}\left(\frac{RH}{\sqrt{1 + R^2 H^2}} \right) \right], \tag{2}$$

where $R = M_\tau\sqrt{(\gamma-1)\,\mathrm{Pr}_t/2}$, $H = B_q/((\gamma-1)M_\tau^2)$, $M_\tau = u_\tau/c_w$, and $B_q = q_w/(\rho_w c_p u_\tau T_w)$. We assume the turbulent Prandtl number is $\mathrm{Pr}_t = 0.87$, and, assuming the Reynolds analogy holds, the heat-flux number is $B_q = c_f\rho_e U_e(T_w - T_r)/(2\,\mathrm{Pr}_e\,\rho_w u_\tau T_w)$.[95]

The transformed KTV- and PIV-derived velocity profiles are presented in Fig. 8 (left). Also, in Fig. 8 (left), we plot the viscous sublayer as $U^+_{VD} = y^+$ as well as applying Eq. 2 to the logarithmic law as

$$U^+_{VD} = \frac{1}{\kappa}\ln(y^+) + C \tag{3}$$

with $\kappa = 0.41$ and $C = 5.2$. The transformed velocity follows the law of the wall in the logarithmic region with good agreement.

In Fig. 8 (right), we present the streamwise velocity fluctuation results that are non-dimensionalized by the Morkovin[96] scaling and compare those to the literature.[29,86,97,98] In this work, we were able to resolve far closer to the wall than in the previous effort by Zahradka et al.[79] The agreement between the fluctuation data from the literature and KTV is good to down to $y/\delta \approx 0.075$.

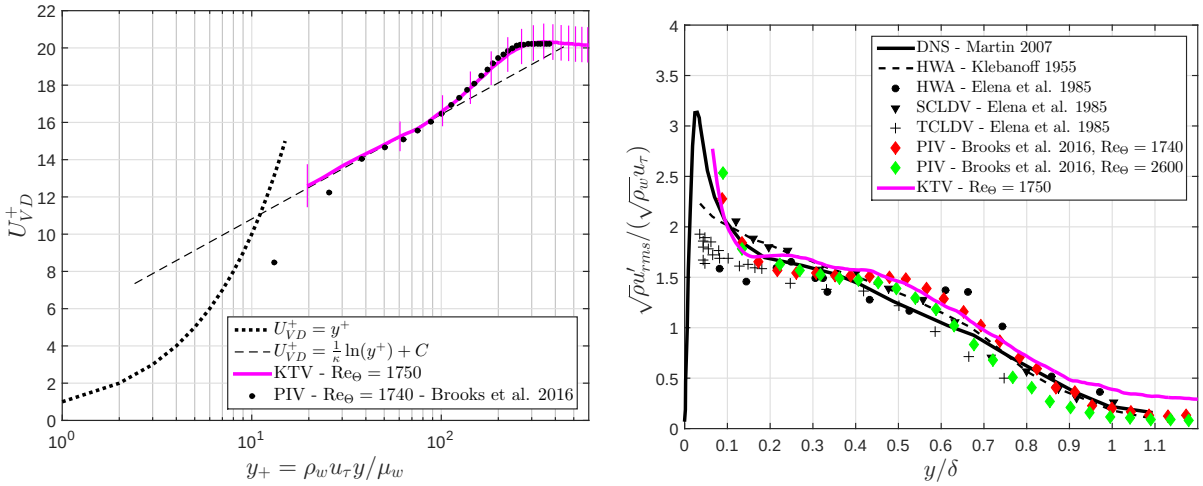

Figure 8. Left: Van Driest scaling of the mean velocity. Right: Morkovin scaling of streamwise fluctuations.

The most significant improvement over the previous KTV work by Zahradka et al.[79] is the ability to write multiple lines. With the ability to write multiple lines, the longitudinal correlation coefficient can be

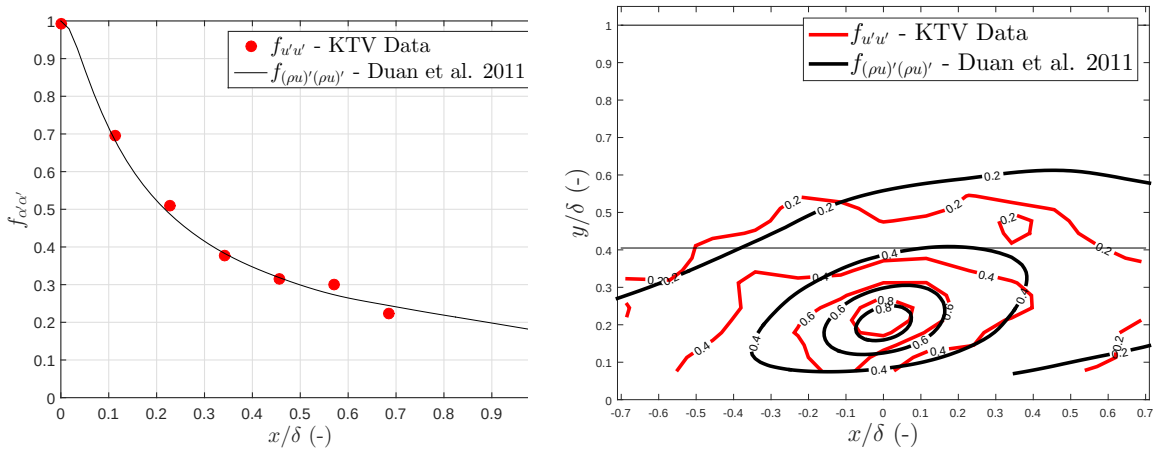

Figure 9. Left: Longitudinal correlation for $y/\delta \approx 0.2$. As a means of first comparison, $f_{u'u'}$ from the present KTV boundary-layer data is compared to $f_{(\rho u)'(\rho u)'}$ from Duan et al.[99] Right: Contours of correlation. Thin horizontal lines mark the boundary-layer edge and approximate wake-region boundary. KTV data in red, DNS data in black.

calculated as

$$f(\mathbf{x}, r) = \frac{\overline{u'(\mathbf{x})u'(\mathbf{x}+r)}}{\overline{u'^2}} = \frac{R_{u'u'}}{\overline{u'^2}} \tag{4}$$

by using the spacing between each write line, r. The longitudinal correlation of the streamwise velocity data are presented as Fig. 9 (left) for $y/\delta \approx 0.2$. As a means of first comparison, $f_{u'u'}$ from the present KTV boundary-layer data is compared to $f_{(\rho u)'(\rho u)'}$ from Duan et al.[99] It should be noted that the work from Duan et al.[99] is at different conditions, $M_\infty = 2.97$, $\mathrm{Re}_\Theta = 3030$.

Moreover, because the flow field should have forwards and backward symmetry, the number of points used for the longitudinal correlation can be increased from 7 to 13 by performing the correlation in Eq. 4 from left-to-right and also right-to-left and concatenating the datasets. This correlation is performed for the field recorded in Fig. 6 for $y/\delta \approx 0.2$ and presented as Fig. 9 (right). Thin horizontal lines in Fig. 9 (right) mark the boundary-layer edge at $y/\delta = 1$ and also the approximate location of the wake-region boundary at $y/\delta \approx 0.41$. Contours of $f_{(\rho u)'(\rho u)'}$ as computed by DNS data from Duan et al[99] are plotted in black, and contours of $f_{u'u'}$ as measured from KTV data are plotted in red. The KTV data have more scatter, as expected, but the orientation of the contours is quite similar indicating that the average angle of turbulent structures is also similar. In future studies, estimates of the structure angle will be made and compared to the literature.

VI. Multi-Line KTV Results With 24-degree Compression Corner in $M_\infty = 2.8$, $\mathbf{Re}_\Theta = 1750$ Flow

The experiments performed in the previous section for the Mach 2.8 boundary layer established the baseline flow characteristics. In this section, we present results of the KTV investigation of the area immediately before a 24-degree compression corner. The experimental setup and data processing routine are the same as that for the boundary layer, except that the write/read delay was changed to 1 µs. The results for seven exposures along with the overlay of the line centers are presented in Fig. 10. The significant increase in turbulence intensity is readily apparent in the flow immediately preceding the compression ramp in Fig. 10 relative to the incoming boundary-layer flow presented in Fig. 6.

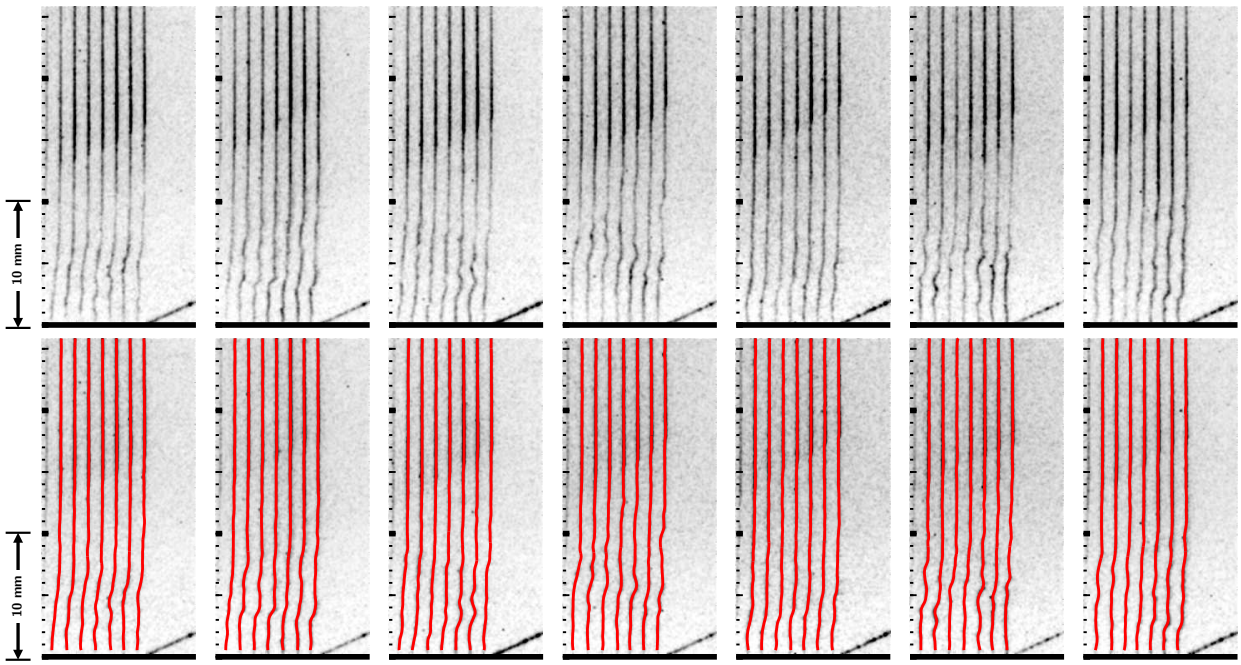

Figure 10. Shock-wave/turbulent-boundary-layer interaction boundary-layer fluorescence exposures for 7 sample frames. Major tick marks are 10 mm. Flow is left to right. Inverted intensity scale. Wall are masked as black. Top: Exposures, Bottom: Exposures with overlay of Gaussian fits to data.

In Fig. 11 (left), the mean velocity for each of the seven write/read pairs in plotted. Each thin vertical black line represents the abscissa origin for a write/read pair. In Fig. 11 (right), the mean velocity is plotted over the mean schlieren exposures, shown previously in Fig. 4. A defect in the velocity profile that is more apparent in the profiles near to the compression corner appears to coincide with the mean shock location.

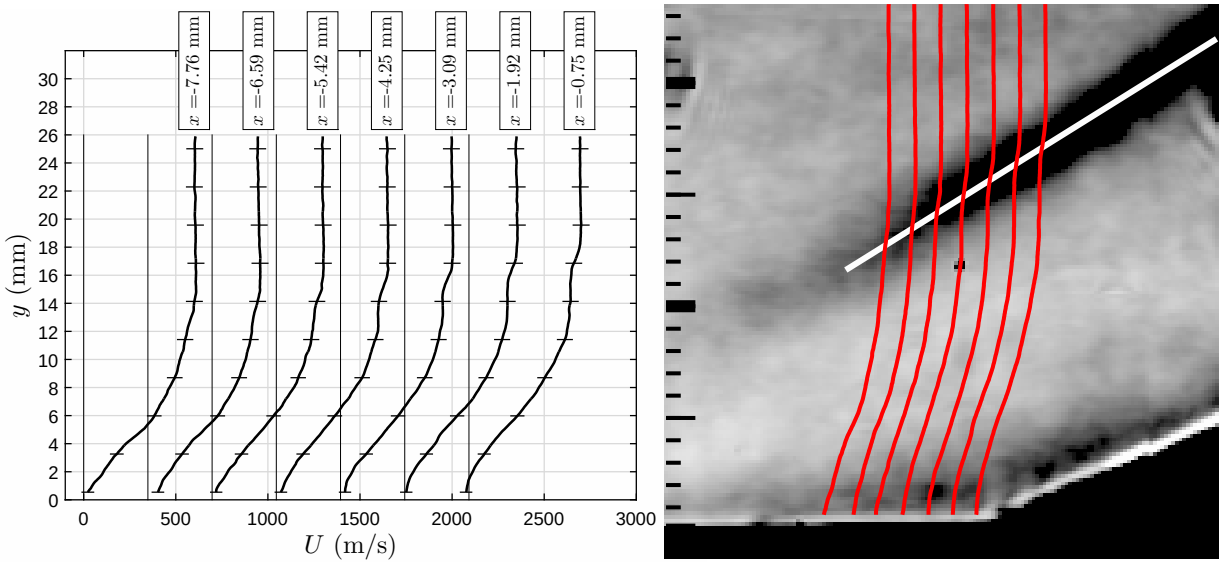

Figure 11. Left: Dimensional velocity of the Mach 2.8 shock-wave/turbulent-boundary-layer interaction. Error bars in black. Thin, vertical lines form ordinates for each profile. Right: Overlay of the mean-velocity measurements with the mean schlieren image. Note the defect in velocity overlaps with the apparent shock location.

The mean velocity for each profile is non-dimesionalized by the freestream velocity and plotted in Fig. 12 (left). Also in this figure are DNS computational results from Priebe and Martin[30] for the wedge of the same geometry, an incoming boundary-layer thickness of 7.1 mm, and a Reynolds number of $\mathrm{Re}_\Theta = 2900$. The agreement between the DNS and the KTV results is excellent except for the approximate shock location at $y/\delta \approx 1.1 - 1.5$. The reason for this disagreement is unclear at the time of this writing.

Profiles of the turbulence intensity in the shock-wave/turbulent boundary-layer interaction normalized by the turbulence intensity of the incoming boundary layer as u'^2_{SWBLI}/u'^2_{BL} are plotted in Fig. 12 (right). There is significant scatter in the data and the amplification falls in the range of 10-20. This is comparable with the data from Fig. 10 of Smits and Muck.[9] In addition, the shock location manifests itself as a slight increase in the fluctuation level at $y/\delta \approx 1.4 - 1.8$.

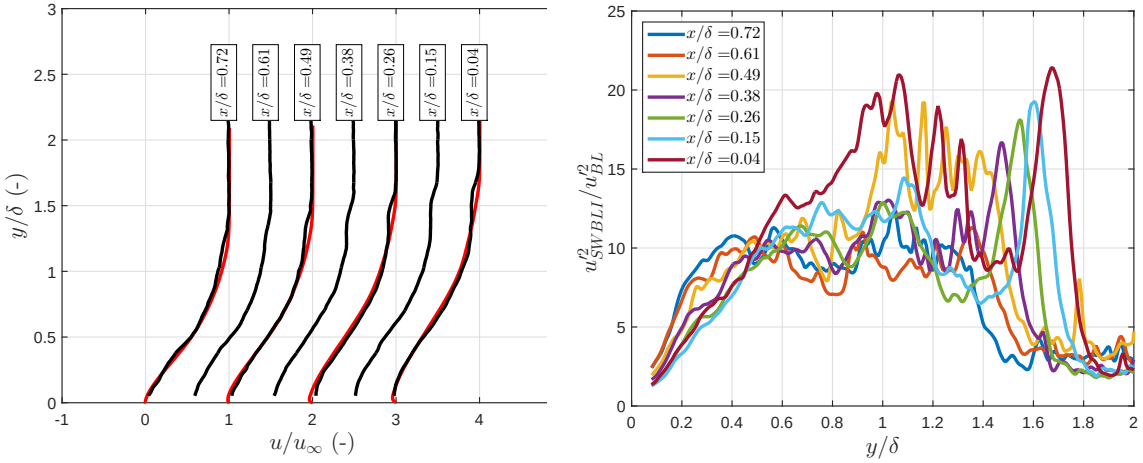

Figure 12. Data for the shock-wave/ boundary-layer interaction. Left: Comparison of the KTV mean velocity (black) with Priebe and Martin[30] (in red). Right: Profiles of the turbulence intensity in the shock-wave/turbulent boundary-layer interaction normalized by the turbulence intensity of the incoming boundary layer as u'^2_{SWBLI}/u'^2_{BL}.

In an additional effort to compare the present KTV results to DNS, a portion of the analysis of the shear layer near the compression corner in Helm et al.[32] is repeated here, but for the experimental KTV data. In Helm et al.,[32] the time-averaged shear layer flow field was analyzed in the context of the mean kinetic energy of the flow, $TKE = (u'^2_{RMS} + v'^2_{RMS})/(2U^2_\infty)$. They used the maximum of the TKE to define a coordinate system in which to normalize the shear layer profiles with the hypothesis that the shear layer profiles would collapse when plotted against a similarity variable. In this work, only streamwise fluctuation data was collected, so only a portion of the TKE can be plotted, $(u'^2_{RMS})/(2U^2_\infty)$; however, it is most likely the maximum of the streamwise fluctuations also marks the center of the shear layer in this flow field. In Fig. 13 (left), the normalized streamwise fluctuations are presented with their maximum values marked by circles. The spatial location of maxima are fitted by linear regression to find the equation of a line, $y = mx+b = \tan(\theta)(x-x_{01})$. Here, θ is the angle of the new coordinate system (x', y') relative to the old coordinate system (x, y), and x_{01} is the x location of the origin of the new coordinate system (x', y'). The coordinate systems are shown with an overlay of $(u'^2_{RMS})/(2U^2_\infty)$ in Fig. 13 (right). The shear layer coordinate system is found to be located at $x_{01}/\delta = -1.7$ at an angle $\theta = 18.8°$. This compares reasonably well with the values of Helm et al.[32] which are reported to be $x_{01}/\delta = -1.9$ at an angle $\theta = 16.5°$.

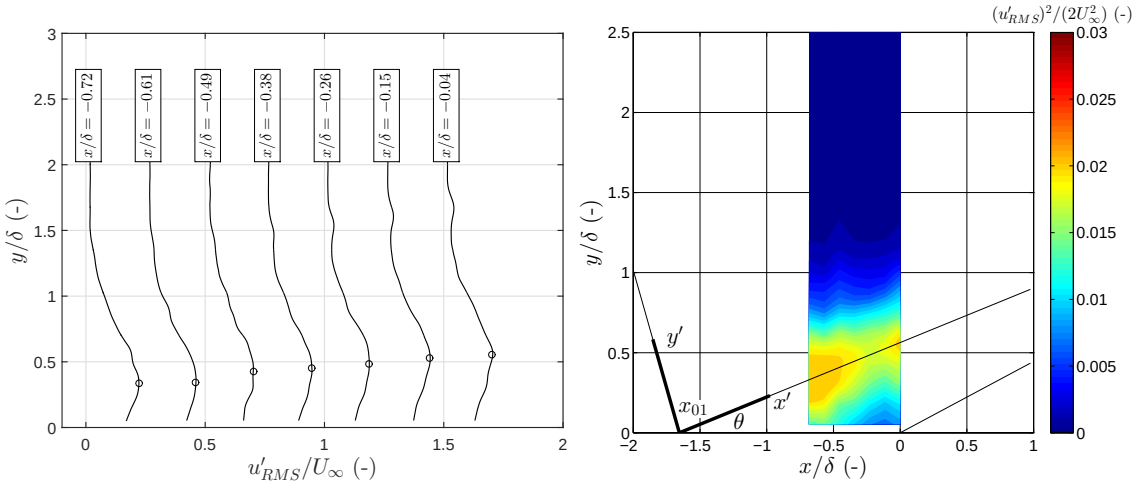

Figure 13. Left: Streamwise fluctuations normalized by the freestream velocity. Local maxima denoted by open circles for each profile. Right: Contour of streamwise fluctuation energy. (x', y') plane defines coordinate system through mean location of shear layer. Black lines normal to x' define interrogation points of interpolated KTV data.

VII. Conclusions and Future Work

Seven profiles of streamwise velocity were measured in the incoming boundary layer and immediately upstream of a 24-degree compression corner in a $M_\infty = 2.8$, $\mathrm{Re}_\Theta = 1750$ shock-wave/turbulent boundary-layer interaction. The measurements were made with Krypton Tagging Velocimetry (KTV) in 99%N_2/1% Kr flow. Globally seeding 1% Kr into the flow (premixed N_2/Kr K-bottles from distributer) alters the major non-dimensional transport properties by 0.1-0.3%.

The mean-velocity and velocity-fluctuation profiles in the incoming supersonic turbulent boundary layer were found to agree with datasets in the literature, thus, the baseline flow was established. Comparisons of the longitudinal correlation as measured by KTV and calculated by DNS are favorable, although, KTV measures u' and the DNS reported $(\rho u)'$. Moreover, contours of $f_{(\rho u)'(\rho u)'}$ as computed by DNS data from Duan et al[99] and $f_{u'u'}$ as measured from KTV data are compared. The KTV data have more scatter, as expected, but the orientation of the contours is quite similar indicating that the average angle of turbulent structures is also similar. Further investigation is warranted.

The mean-velocity profiles in the region immediately upstream of the compression corner were found to agree with Direct Numerical Simulation (DNS) results available in the literature. Other means of comparison of the present experimental results to other experiments and calculations will be pursued in the future.

One takeaway from this effort is that tagging velocimetry may be used successfully in complex flowfields,

such as shock-wave/turbulent boundary-layer interactions. Favorable comparison of the KTV measurements to other datasets should enable confidence in applying tagging velocimetry to other flow fields where alternative methods of measurement are more difficult. One contrasting form of measurement is Particle Image Velocimetry (PIV), which is limited by a fundamental particle-response issue. Moreover, KTV, relative to other tagging velocimetry techniques, relies on an inert chemical tracer which should enable implementation in flow fields where the thermochemical state is difficult to prescribe or predict.

Multi-line KTV results were presented in this work that quantified streamwise velocity only. A natural extension to this is to write a grid for two-dimensional KTV. The equipment used for the current effort should have sufficient capability to accomplish this goal. Moreover, different re-excitation schemes and camera lenses will be investigated in the pursuit of higher SNR.

Acknowledgments

The M3CT facilities were supplied by the Arnold Engineering Development Complex (AEDC). The Air Force SFFP supported Hunt and Parziale with a stipend for this work. Mustafa and Parziale were supported by AFOSR Young Investigator Program Grant FA9550-16-1-0262 and equipment for this work was supported by AFOSR DURIP Grant FA9550-15-1-0325, for both of which Ivett Leyva is the Program Manager. We would like to acknowledge the encouragement of John Laffery and Dan Marren of AEDC White Oak. The authors would like to thank Jon Brooks for his technical help running the M3CT and sharing PIV data. The authors would like to thank Pino Martin for sharing DNS data. The authors would like to thank Stuart Laurence and Ken Yu for permitting us to use the Phantom camera and Cavilux light source.

References

[1]Woolf, A. F., "Conventional Prompt Global Strike and Long-Range Ballistic Missiles: Background and Issues," R41464, 2016, Congressional Research Service.

[2]Acton, J. M., "Silver Bullet? Asking the Right Questions About Conventional Prompt Global Strike," CPGS, 2013, Carnegie Endowment for International Peace.

[3]Acton, J. M., "Hypersonic Boost-Glide Weapons," *Science & Global Security*, Vol. 23, No. 3, 2015, pp. 191–219. doi: 10.1080/08929882.2015.1087242.

[4]Dolling, D. S., "Fifty Years of Shock-Wave/Boundary-Layer Interaction Research: What next?" *AIAA Journal*, Vol. 39, No. 8, 2001, pp. 1517–1531. doi: 10.2514/2.1476.

[5]Settles, G. S., Vas, I. E., and Bogdonoff, S. M., "Details of a Shock-Separated Turbulent Boundary Layer at a Compression Corner," *AIAA Journal*, Vol. 14, No. 12, 1976, pp. 1709–1715. doi: 10.2514/3.61513.

[6]Settles, G. S., Fitzpatrick, T. J., and Bogdonoff, S. M., "Detailed Study of Attached and Separated Compression Corner Flowfields in High Reynolds Number Supersonic Flow," *AIAA Journal*, Vol. 17, No. 6, 1979, pp. 579–585. doi: 10.2514/3.61180.

[7]Dolling, D. S. and Murphy, M. T., "Unsteadiness of the Separation Shock Wave Structure in a Supersonic Compression Ramp Flowfield," *AIAA Journal*, Vol. 21, No. 12, 1983, pp. 1628–1634. doi: 10.2514/3.60163.

[8]Kuntz, D. W., Amatucci, V. A., and Addy, A. L., "Turbulent Boundary-Layer Properties Downstream of the Shock-Wave/Boundary-Layer Interaction," *AIAA journal*, Vol. 25, No. 5, 1987, pp. 668–675. doi: 10.2514/3.9681.

[9]Smits, A. J. and Muck, K.-C., "Experimental study of three shock wave/turbulent boundary layer interactions," *Journal of Fluid Mechanics*, Vol. 182, 1987, pp. 291–314. doi: 10.1017/S0022112087002349.

[10]Selig, M. S., Andreopoulos, J., Muck, K. C., Dussauge, J. P., and Smits, A. J., "Turbulence Structure in a Shock Wave/Turbulent Boundary-Layer Interaction," *AIAA Journal*, Vol. 27, No. 7, 1989, pp. 862–869. doi: 10.2514/3.10193.

[11]Brusniak, L. and Dolling, D. S., "Physics of unsteady blunt-fin-induced shock wave/turbulent boundary layer interactions," *Journal of Fluid Mechanics*, Vol. 273, 1994, pp. 375–409. doi: 10.1017/S0022112094001989.

[12]Andreopoulos, Y., Agui, J. H., and Briassulis, G., "Shock Wave-Turbulence Interactions," *Annual Review of Fluid Mechanics*, Vol. 32, No. 1, 2000, pp. 309–345. doi: 10.1146/annurev.fluid.32.1.309.

[13]Wu, P., Lempert, W. L., and Miles, R. B., "Megahertz Pulse-Burst Laser and Visualization of Shock-Wave/Boundary-Layer Interaction," *AIAA Journal*, Vol. 38, No. 4, 2000, pp. 672–679. doi: 10.2514/2.1009.

[14]Wu, P. P. and Miles, R. B., "Megahertz Visualization of Compression-Corner Shock Structures," *AIAA Journal*, Vol. 39, No. 8, 2001, pp. 1542–1546. doi: 10.2514/2.1478.

[15]Beresh, S. J., Clemens, N. T., and Dolling, D. S., "Relationship Between Upstream Turbulent Boundary-Layer Velocity Fluctuations and Separation Shock Unsteadiness," *AIAA Journal*, Vol. 40, No. 12, 2002, pp. 2412–2422. doi: 10.2514/2.1609.

[16]Bookey, P., Wyckham, C., Smits, A., and Martin, M. P., "New Experimental Data of STBLI at DNS/LES Accessible Reynolds Numbers," *Proceedings of 43rd AIAA Aerospace Sciences Meeting and Exhibit*, AIAA-2005-309, Reno, Nevada, 2005. doi: 10.2514/6.2005-309.

[17]Dupont, P., Haddad, C., Ardissone, J., and Debiève, J. F., "Space and time organisation of a shock wave/turbulent boundary layer interaction," *Aerospace Science and Technology*, Vol. 9, No. 7, 2005, pp. 561–572. doi: 10.1016/j.ast.2004.12.009.

[18]Dupont, P., Haddad, C., and Debiève, J. F., "Space and time organization in a shock-induced separated boundary layer," *Journal of Fluid Mechanics*, Vol. 559, 2006, pp. 255–277. doi: 10.1017/S0022112006000267.

[19]Ganapathisubramani, B., Clemens, N. T., and Dolling, D. S., "Effects of upstream boundary layer on the unsteadiness of shock-induced separation," *Journal of Fluid Mechanics*, Vol. 585, 2007, pp. 369–394. doi: 10.1017/S0022112007006799.

[20]Humble, R. A., Scarano, F., and van Oudheusden, B. W., "Particle image velocimetry measurements of a shock wave/turbulent boundary layer interaction," *Experiments in Fluids*, Vol. 43, No. 2-3, 2007, pp. 173–183. doi: 10.1007/s00348-007-0337-8.

[21]Humble, R. A., Elsinga, G. E., Scarano, F., and van Oudheusden, B. W., "Three-dimensional instantaneous structure of a shock wave/turbulent boundary layer interaction," *Journal of Fluid Mechanics*, Vol. 622, 2009, pp. 33–62. doi: 10.1017/S0022112008005090.

[22]Ringuette, M. J., Bookey, P., Wyckham, C., and Smits, A. J., "Experimental Study of a Mach 3 Compression Ramp Interaction at $Re_\Theta = 2400$," *AIAA Journal*, Vol. 47, No. 2, 2009, pp. 373–385. doi: 10.2514/1.38248.

[23]Murray, N., Hillier, R., and Williams, S., "Experimental investigation of axisymmetric hypersonic shock-wave/turbulent-boundary-layer interactions," *Journal of Fluid Mechanics*, Vol. 714, 2013, pp. 152–189. doi: 10.1017/jfm.2012.464.

[24]Adams, N. A., "Direct simulation of the turbulent boundary layer along a compression ramp at $M = 3$ and $Re_\Theta = 1685$," *Journal of Fluid Mechanics*, Vol. 420, 2000, pp. 47–83. doi: 10.1017/S0022112000001257.

[25]Xu, S. and Martin, M. P., "Assessment of inflow boundary conditions for compressible turbulent boundary layers," *Physics of Fluids*, Vol. 16, No. 7, 2004, pp. 2623–2639. doi: 10.1063/1.1758218.

[26]Martin, M. P. and Candler, G. V., "A parallel implicit method for the direct numerical simulation of wall-bounded compressible turbulence," *Journal of Computational Physics*, Vol. 215, No. 1, 2006, pp. 153–171. doi: doi:10.1016/j.jcp.2005.10.017.

[27]Wu, M. and Martin, M. P., "Direct Numerical Simulation of Supersonic Turbulent Boundary Layer Over a Compression Ramp," *AIAA Journal*, Vol. 45, No. 4, 2007, pp. 879–889. doi: 10.2514/1.27021.

[28]Wu, M. and Martin, M. P., "Analysis of shock motion in shockwave and turbulent boundary layer interaction using direct numerical simulation data," *Journal of Fluid Mechanics*, Vol. 594, 2008, pp. 71–83. doi: 10.1017/S0022112007009044.

[29]Martin, M. P., "Direct numerical simulation of hypersonic turbulent boundary layers. Part 1. Initialization and comparison with experiments," *Journal of Fluid Mechanics*, Vol. 570, 2007, pp. 347–364. doi: 10.1017/S0022112006003107.

[30]Priebe, S. and Martin, M. P., "Low-frequency unsteadiness in shock wave–turbulent boundary layer interaction," *Journal of Fluid Mechanics*, Vol. 699, 2012, pp. 1–49. doi: 10.1017/jfm.2011.560.

[31]Grilli, M., Schmid, P. J., Hickel, S., and Adams, N. A., "Analysis of unsteady behaviour in shockwave turbulent boundary layer interaction," *Journal of Fluid Mechanics*, Vol. 700, 2012, pp. 16–28. doi: 10.1017/jfm.2012.37.

[32]Helm, C., Martin, M. P., and Dupont, P., "Characterization of the shear layer in a Mach 3 shock/turbulent boundary layer interaction," *Journal of Physics: Conference Series*, Vol. 506, No. 1, 2014, pp. 012013. doi: 10.1088/1742-6596/506/1/012013.

[33]Settles, G. S. and Bogdonoff, S. M., "Scaling of Two- and Three-Dimensional Shock/Turbulent Boundary-Layer Interactions at Compression Corners," *AIAA Journal*, Vol. 20, No. 6, 1982, pp. 782–789. doi: 10.2514/3.51135.

[34]Settles, G. S. and, D. L. J., "Hypersonic Shock/Boundary-Layer Interaction Database: New and Corrected Data," NASA CR 177638, 1994.

[35]Knight, D., Yan, H., Panaras, A. G., and Zheltovodov, A., "Advances in CFD prediction of shock wave turbulent boundary layer interactions," *Progress in Aerospace Sciences*, Vol. 39, No. 2, 2003, pp. 121–184. doi: 10.1016/S0376-0421(02)00069-6.

[36]Dussauge, J.-P. and Piponniau, S., "Shock/boundary-layer interactions: Possible sources of unsteadiness," *Journal of Fluids and Structures*, Vol. 24, No. 8, 2008, pp. 1166–1175. doi: 10.1016/j.jfluidstructs.2008.06.003.

[37]Babinsky, H. and Harvey, J. K., editors, *Shock Wave-Boundary-Layer Interactions*, Cambridge University Press, 1st ed., 2011.

[38]Clemens, N. T. and Narayanaswamy, V., "Low-Frequency Unsteadiness of Shock Wave/Turbulent Boundary Layer Interactions," *Annual Review of Fluid Mechanics*, Vol. 46, 2014, pp. 469–492. doi: 10.1146/annurev-fluid-010313-141346.

[39]Gaitonde, D. V., "Progress in shock wave/boundary layer interactions," *Progress in Aerospace Sciences*, Vol. 72, 2015, pp. 80–99. doi: 10.1016/j.paerosci.2014.09.002.

[40]Gnoffo, P. A., Berry, S. A., and Van Norman, J. W., "Uncertainty Assessments of Hypersonic Shock Wave-Turbulent Boundary-Layer Interactions at Compression Corners," *Journal of Spacecraft and Rockets*, Vol. 50, No. 1, 2013, pp. 69–95. doi: 10.2514/1.A32250.

[41]Haertig, J., Havermann, M., Rey, C., and George, A., "Particle Image Velocimetry in Mach 3.5 and 4.5 Shock-Tunnel Flows," *AIAA Journal*, Vol. 40, No. 6, 2002, pp. 1056–1060. doi: 10.2514/2.1787.

[42]Loth, E., "Compressibility and Rarefaction Effects on Drag of a Spherical Particle," *AIAA Journal*, Vol. 46, No. 9, 2008, pp. 2219–2228. doi: 10.2514/1.28943.

[43]Koochesfahani, M. M. and Nocera, D. G., "Molecular Tagging Velocimetry," *Springer Handbook of Experimental Fluid Mechanics*, edited by Tropea, C. and Yarin, A. L. and Foss, J. F., Springer, 2007.

[44]Hsu, A. G., Srinivasan, R., Bowersox, R. D. W., and North, S. W., "Molecular Tagging Using Vibrationally Excited Nitric Oxide in an Underexpanded Jet Flowfield," *AIAA Journal*, Vol. 47, No. 11, 2009, pp. 2597–2604. doi: 10.2514/1.39998.

[45]Hsu, A. G., Srinivasan, R., Bowersox, R. D. W., and North, S. W., "Two-component molecular tagging velocimetry utilizing NO fluorescence lifetime and NO_2 photodissociation techniques in an underexpanded jet flowfield," *Applied Optics*, Vol. 48, No. 22, 2009, pp. 4414–4423. doi: 10.1364/AO.48.004414.

[46]Sánchez-González, R., Srinivasan, R., Bowersox, R. D. W., and North, S. W., "Simultaneous velocity and temperature measurements in gaseous flow fields using the VENOM technique," *Optics Letters*, Vol. 36, No. 2, 2011, pp. 196–198. doi: 10.1364/OL.36.000196.

[47]Sánchez-González, R., Bowersox, R. D. W., and North, S. W., "Simultaneous velocity and temperature measurements in gaseous flowfields using the vibrationally excited nitric oxide monitoring technique: a comprehensive study," *Applied Optics*, Vol. 51, No. 9, 2012, pp. 1216–1228. doi: 10.1364/AO.51.001216.

[48]Sánchez-González, R., Bowersox, R. D. W., and North, S. W., "Vibrationally excited NO tagging by NO($A^2\Sigma^+$) fluorescence and quenching for simultaneous velocimetry and thermometry in gaseous flows," *Optics Letters*, Vol. 39, No. 9, 2014, pp. 2771–2774. doi: 10.1364/OL.39.002771.

[49]Dam, N., Klein-Douwel, R. J. H., Sijtsema, N. M., and ter Meulen, J. J., "Nitric oxide flow tagging in unseeded air," *Optics Letters*, Vol. 26, No. 1, 2001, pp. 36–38. doi: 10.1364/OL.26.000036.

[50]Sijtsema, N. M., Dam, N. J., Klein-Douwel, R. J. H., and ter Meulen, J. J., "Air Photolysis and Recombination Tracking: A New Molecular Tagging Velocimetry Scheme," *AIAA Journal*, Vol. 40, No. 6, 2002, pp. 1061–1064. doi: 10.2514/2.1788.

[51]Van der Laan, W. P. N., Tolboom, R. A. L., Dam, N. J., and ter Meulen, J. J., "Molecular tagging velocimetry in the wake of an object in supersonic flow," *Experiments in Fluids*, Vol. 34, No. 4, 2003, pp. 531–534. doi: 10.1007/s00348-003-0593-1.

[52]Miles, R., Cohen, C., Connors, J., Howard, P., Huang, S., Markovitz, E., and Russell, G., "Velocity measurements by vibrational tagging and fluorescent probing of oxygen," *Optics Letters*, Vol. 12, No. 11, 1987, pp. 861–863. doi: 10.1364/OL.12.000861.

[53]Miles, R., Connors, J., Markovitz, E., Howard, P., and Roth, G., "Instantaneous profiles and turbulence statistics of supersonic free shear layers by Raman excitation plus laser-induced electronic fluorescence (RELIEF) velocity tagging of oxygen," *Experiments in Fluids*, Vol. 8, No. 1-2, 1989, pp. 17–24. doi: 10.1007/BF00203060.

[54]Miles, R. B., Zhou, D., Zhang, B., and Lempert, W. R., "Fundamental Turbulence Measurements by RELIEF Flow Tagging," *AIAA Journal*, Vol. 31, No. 3, 1993, pp. 447–452. doi: 10.2514/3.11350.

[55]Miles, R. B. and Lempert, W. R., "Quantitative Flow Visualization in Unseeded Flows," *Annual Review of Fluid Mechanics*, Vol. 29, No. 1, 1997, pp. 285–326. doi: 10.1146/annurev.fluid.29.1.285.

[56]Miles, R. B., Grinstead, J., Kohl, R. H., and Diskin, G., "The RELIEF flow tagging technique and its application in engine testing facilities and for helium-air mixing studies," *Measurement Science and Technology*, Vol. 11, No. 9, 2000, pp. 1272–1281. doi: 10.1088/0957-0233/11/9/304.

[57]Michael, J. B., Edwards, M. R., Dogariu, A., and Miles, R. B., "Femtosecond laser electronic excitation tagging for quantitative velocity imaging in air," *Applied Optics*, Vol. 50, No. 26, 2011, pp. 5158–5162. doi: 10.1364/AO.50.005158.

[58]Edwards, M. R., Dogariu, A., and Miles, R. B., "Simultaneous Temperature and Velocity Measurements in Air with Femtosecond Laser Tagging," *AIAA Journal*, Vol. 53, No. 8, 2015, pp. 2280–2288. doi: 10.2514/1.J053685.

[59]Jiang, N., Halls, B. R., Stauffer, H. U., Danehy, P. M., Gord, J. R., and Roy, S., "Selective two-photon absorptive resonance femtosecond-laser electronic-excitation tagging velocimetry," *Optics Letters*, Vol. 41, No. 10, 2016, pp. 2225–2228. doi: 10.1364/OL.41.002225.

[60]Jiang, N., Mance, J. G., Slipchenko, M. N., Felver, J. J., Stauffer, H. U., Yi, T., Danehy, P. M., and Roy, S., "Seedless velocimetry at 100 kHz with picosecond-laser electronic-excitation tagging," *Optics Letters*, Vol. 42, No. 2, 2017, pp. 239–242. doi: 10.1364/OL.42.000239.

[61]McDaniel, J. C., Hiller, B., and Hanson, R. K., "Simultaneous multiple-point velocity measurements using laser-induced iodine fluorescence," *Optics Letters*, Vol. 8, No. 1, 1983, pp. 51–53. doi: 10.1364/OL.8.000051.

[62]Balla, R. J., "Iodine Tagging Velocimetry in a Mach 10 Wake," *AIAA Journal*, Vol. 51, No. 7, 2013, pp. 1–3. doi: 10.2514/1.J052416.

[63]Lempert, W. R., Jiang, N., Sethuram, S., and Samimy, M., "Molecular Tagging Velocimetry Measurements in Supersonic Microjets," *AIAA Journal*, Vol. 40, No. 6, 2002, pp. 1065–1070. doi: 10.2514/2.1789.

[64]Lempert, W. R., Boehm, M., Jiang, N., Gimelshein, S., and Levin, D., "Comparison of molecular tagging velocimetry data and direct simulation Monte Carlo simulations in supersonic micro jet flows," *Experiments in Fluids*, Vol. 34, No. 3, 2003, pp. 403–411. doi: 10.1007/s00348-002-0576-7.

[65]Handa, T., Mii, K., Sakurai, T., Imamura, K., Mizuta, S., and Ando, Y., "Study on supersonic rectangular microjets using molecular tagging velocimetry," *Experiments in Fluids*, Vol. 55, No. 5, 2014, pp. 1–9. doi: 10.1007/s00348-014-1725-5.

[66]Boedeker, L. R., "Velocity measurement by H_2O photolysis and laser-induced fluorescence of OH," *Optics Letters*, Vol. 14, No. 10, 1989, pp. 473–475. doi: 10.1364/OL.14.000473.

[67]Wehrmeyer, J. A., Ribarov, L. A., Oguss, D. A., and Pitz, R. W., "Flame Flow Tagging Velocimetry with 193-nm H_2O Photodissociation," *Applied Optics*, Vol. 38, No. 33, 1999, pp. 6912–6917. doi: 10.1364/AO.38.006912.

[68]Pitz, R. W., Lahr, M. D., Douglas, Z. W., Wehrmeyer, J. A., Hu, S., Carter, C. D., Hsu, K.-Y., Lum, C., and Koochesfahani, M. M., "Hydroxyl tagging velocimetry in a supersonic flow over a cavity," *Applied Optics*, Vol. 44, No. 31, 2005, pp. 6692–6700. doi: 10.1364/AO.44.006692.

[69]Hiller, B., Booman, R. A., Hassa, C., and Hanson, R. K., "Velocity visualization in gas flows using laser-induced phosphorescence of biacetyl," *Review of Scientific Instruments*, Vol. 55, No. 12, 1984, pp. 1964–1967. doi: 10.1063/1.1137687.

[70]Gendrich, C. P. and Koochesfahani, M. M., "A spatial correlation technique for estimating velocity fields using molecular tagging velocimetry (MTV)," *Experiments in Fluids*, Vol. 22, No. 1, 1996, pp. 67–77. doi: 10.1007/BF01893307.

[71]Gendrich, C. P., Koochesfahani, M. M., and Nocera, D. G., "Molecular tagging velocimetry and other novel applications of a new phosphorescent supramolecule," *Experiments in Fluids*, Vol. 23, No. 5, 1997, pp. 361–372. doi: 10.1007/s003480050123.

[72]Stier, B. and Koochesfahani, M. M., "Molecular tagging velocimetry (MTV) measurements in gas phase flows," *Experiments in Fluids*, Vol. 26, No. 4, 1999, pp. 297–304. doi: 10.1007/s003480050292.

[73]Ribarov, L. A., Wehrmeyer, J. A., Batliwala, F., Pitz, R. W., and DeBarber, P. A., "Ozone Tagging Velocimetry Using Narrowband Excimer Lasers," *AIAA Journal*, Vol. 37, No. 6, 1999, pp. 708–714. doi: 10.2514/2.799.

[74]Mills, J. L., Sukenik, C. I., and Balla, R. J., "Hypersonic Wake Diagnostics Using Laser Induced Fluorescence Techniques," *Proceedings of 42nd AIAA Plasmadynamics and Lasers Conference*, AIAA 2011-3459, Honolulu, Hawaii, 2011. doi: 10.2514/6.2011-3459.

[75]Balla, R. J. and Everhart, J. L., "Rayleigh Scattering Density Measurements, Cluster Theory, and Nucleation Calculations at Mach 10," *AIAA Journal*, Vol. 50, No. 3, 2012, pp. 698–707. doi: 10.2514/1.J051334.

[76]Parziale, N. J., Smith, M. S., and Marineau, E. C., "Krypton Tagging Velocimetry for Use in High-Speed Ground-Test Facilities," *Proceedings of AIAA SciTech 2015*, AIAA-2015-1484, Kissimmee, Florida, 2015. doi: 10.2514/6.2015-1484.

[77]Parziale, N. J., Smith, M. S., and Marineau, E. C., "Krypton tagging velocimetry of an underexpanded jet," *Applied Optics*, Vol. 54, No. 16, 2015, pp. 5094–5101. doi: 10.1364/AO.54.005094.

[78]Zahradka, D., Parziale, N. J., Smith, M. S., and Marineau, E. C., "Krypton Tagging Velocimetry (KTV) in Supersonic Turbulent Boundary Layers," *Proceedings of AIAA SciTech 2016*, AIAA-2016-1587, San Diego, California, 2016. doi: 10.2514/6.2016-1587.

[79]Zahradka, D., Parziale, N. J., Smith, M. S., and Marineau, E. C., "Krypton tagging velocimetry in a turbulent Mach 2.7 boundary layer," *Experiments in Fluids*, Vol. 57, No. 62, 2016. doi: 10.1007/s00348-016-2148-2.

[80]Chang, R. S. F., Horiguchi, H., and Setser, D. W., "Radiative lifetimes and twobody collisional deactivation rate constants in argon for Kr($4p^55p$) and Kr($4p^55p$) states," *The Journal of Chemical Physics*, Vol. 73, No. 2, 1980, pp. 778–790. doi: 10.1063/1.440185.

[81]Marren, D. and Lafferty, J., "The AEDC Hypervelocity Wind Tunnel 9," *Advanced Hypersonic Test Facilities*, American Institute of Aeronautics and Astronautics, 2002, pp. 467–478. doi: 10.2514/5.9781600866678.0467.0478.

[82]Settles, G. S., *Schlieren and Shadowgraph Techniques*, Springer-Verlag Berlin Heidelberg, First ed., 2001.

[83]Narayanaswamy, V., Burns, R., and Clemens, N. T., "Kr-PLIF for scalar imaging in supersonic flows," *Optics Letters*, Vol. 36, No. 21, 2011, pp. 4185–4187. doi: 10.1364/OL.36.004185.

[84]Brooks, J., Gupta, A., Smith, M. S., and Marineau, E. C., "Development of Non-Intrusive Velocity Measurement Capabilities at AEDC Tunnel 9," *Proceedings of 52nd Aerospace Sciences Meeting, SciTech*, AIAA-2014-1239, National Harbor, Maryland, 2014. doi: 10.2514/6.2014-1239.

[85]Brooks, J. M., Gupta, A. K., Smith, M. S., and Marineau, E. C., "Development of Particle Image Velocimetry in a Mach 2.7 Wind Tunnel at AEDC White Oak," *Proceedings of 53nd Aerospace Sciences Meeting, SciTech*, AIAA-2015-1915, Kissimmee, Florida, 2015. doi: 10.2514/6.2015-1915.

[86]Brooks, J. M., Gupta, A. K., Smith, M. S., and Marineau, E. C., "PIV Measurements of Mach 2.7 Turbulent Boundary Layer with varying Reynolds Numbers," *Proceedings of 54th Aerospace Sciences Meeting, SciTech*, AIAA-2016-1147, San Diego, California, 2016. doi: 10.2514/6.2016-1147.

[87]Arisman, C. J., Johansen, C. T., Bathel, B. F., and Danehy, P. M., "Investigation of Gas Seeding for Planar Laser-Induced Fluorescence in Hypersonic Boundary Layers," *AIAA Journal*, Vol. 53, No. 12, 2015, pp. 3637–3651. doi: 10.2514/1.J053892.

[88]O'Haver, T., *A Pragmatic Introduction to Signal Processing*, University of Maryland at College Park, 1997.

[89]Bathel, B. F., Danehy, P. M., Inman, J. A., Jones, S. B., Ivey, C. B., and Goyne, C. P., "Velocity Profile Measurements in Hypersonic Flows Using Sequentially Imaged Fluorescence-Based Molecular Tagging," *AIAA Journal*, Vol. 49, No. 9, 2011, pp. 1883–1896. doi: 10.2514/1.J050722.

[90]Whitehead, C. A., Pournasr, H., Bruce, M. R., Cai, H., Kohel, J., Layne, W. B., and Keto, J. W., "Deactivation of two-photon excited Xe($5p^56p$,6p',7p) and Kr($4p^55p$) in xenon and krypton," *The Journal of Chemical Physics*, Vol. 102, No. 5, 1995, pp. 1965–1980. doi: 10.1063/1.468763.

[91]Dzierega, K., Volz, U., Nave, G., and Griesmann, U., "Accurate transition rates for the 5p-5s transitions in Kr I," *Physical Review A*, Vol. 62, No. 2, 2000, pp. 022505. doi: 10.1103/PhysRevA.62.022505.

[92]Hill, R. B. and Klewicki, J. C., "Data reduction methods for flow tagging velocity measurements," *Experiments in Fluids*, Vol. 20, No. 3, 1996, pp. 142–152. doi: 10.1007/BF00190270.

[93]Bradshaw, P., "Compressible Turbulent Shear Layers," *Annual Review of Fluid Mechanics*, Vol. 9, No. 1, 1977, pp. 33–52. doi: 10.1146/annurev.fl.09.010177.000341.

[94]Huang, P. G. and Coleman, G. N., "Van Driest Transformation and Compressible Wall-Bounded Flows," *AIAA Journal*, Vol. 32, No. 10, 1994, pp. 2110–2113. doi: 10.2514/3.12259.

[95]Schlichting, H., *Boundary-Layer Theory*, Springer, 2000.

[96]Morkovin, M. V., "Effects of compressibility on turbulent flows," *Mécanique de la Turbulence*, 1962, pp. 367–380, CNRS.

[97]Klebanoff, P. S., "Characteristics of Turbulence in a Boundary Layer with Zero Pressure Gradient," NACA TR-1247, 1955.

[98]Elena, M., Lacharme, J. P., and Gaviglio, J., "Comparison of hot-wire and laser Doppler anemometry methods in supersonic turbulent boundary layers," *Proceedings of 2nd International Symposium on Laser Anemometry*, Miami Beach, Florida, 1985, pp. 151–157.

[99]Duan, L., Beekman, I., and Martin, M. P., "Direct numerical simulation of hypersonic turbulent boundary layers. Part 3. Effect of Mach number," *Journal of Fluid Mechanics*, Vol. 672, 2011, pp. 245–267. doi: 10.1017/S0022112010005902.